



HAL
open science

Multi-species measurements of nitrogen isotopic composition reveal the spatial constraints and biological drivers of ammonium attenuation across a highly contaminated groundwater system

Naomi S. Wells, Vivien Hakoun, Serge Brouyère, Kay Knöller

► To cite this version:

Naomi S. Wells, Vivien Hakoun, Serge Brouyère, Kay Knöller. Multi-species measurements of nitrogen isotopic composition reveal the spatial constraints and biological drivers of ammonium attenuation across a highly contaminated groundwater system. *Water Research*, 2016, 98, pp.363-375. 10.1016/j.watres.2016.04.025 . hal-01306976

HAL Id: hal-01306976

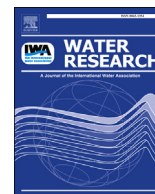
<https://hal.science/hal-01306976>

Submitted on 26 Apr 2016

HAL is a multi-disciplinary open access archive for the deposit and dissemination of scientific research documents, whether they are published or not. The documents may come from teaching and research institutions in France or abroad, or from public or private research centers.

L'archive ouverte pluridisciplinaire **HAL**, est destinée au dépôt et à la diffusion de documents scientifiques de niveau recherche, publiés ou non, émanant des établissements d'enseignement et de recherche français ou étrangers, des laboratoires publics ou privés.

Copyright



Multi-species measurements of nitrogen isotopic composition reveal the spatial constraints and biological drivers of ammonium attenuation across a highly contaminated groundwater system



Naomi S. Wells^{a,*}, Vivien Hakoun^{b,1}, Serge Brouyère^b, Kay Knöller^a

^a Department of Catchment Hydrology, Helmholtz Centre for Environmental Research – UFZ, Theodor-Lieser Str. 4, 06112 Halle (Saale), Germany

^b Université de Liège, Département ArGenCo, Hydrogéologie et Géologie de l'Environnement, Bât. B52/3 – Sart-Tilman, B-4000 Liege, Belgium

ARTICLE INFO

Article history:

Received 14 December 2015

Received in revised form

28 March 2016

Accepted 13 April 2016

Keywords:

Ammonium attenuation

Groundwater

Industrial pollution

Nitrate reduction

Nitrite reduction

Stable isotopes

ABSTRACT

Groundwater under industrial sites is characterised by heterogeneous chemical mixtures, making it difficult to assess the fate and transport of individual contaminants. Quantifying the *in-situ* biological removal (attenuation) of nitrogen (N) is particularly difficult due to its reactivity and ubiquity. Here a multi-isotope approach is developed to distinguish N sources and sinks within groundwater affected by complex industrial pollution. Samples were collected from 70 wells across the two aquifers underlying a historic industrial area in Belgium. Below the industrial site the groundwater contained up to 1000 mg N l⁻¹ ammonium (NH₄⁺) and 300 mg N l⁻¹ nitrate (NO₃⁻), while downgradient concentrations decreased to ~1 mg l⁻¹ DIN ([DIN] = [NH₄⁺-N] + [NO₃⁻-N] + [NO₂⁻-N]). Mean δ¹⁵N-DIN increased from ~2‰ to +20‰ over this flow path, broadly confirming that biological N attenuation drove the measured concentration decrease. Multi-variate analysis of water chemistry identified two distinct NH₄⁺ sources (δ¹⁵N-NH₄⁺ from -14‰ and +5‰) within the contaminated zone of both aquifers. Nitrate dual isotopes co-varied (δ¹⁵N: -3‰ - +60‰; δ¹⁸O: 0‰ - +50‰) within the range expected for coupled nitrification and denitrification of the identified sources. The fact that δ¹⁵N-NO₂⁻ values were 50‰–20‰ less than δ¹⁵N-NH₄⁺ values in the majority of wells confirmed that nitrification controlled N turnover across the site. However, the fact that δ¹⁵N-NO₂⁻ was greater than δ¹⁵N-NH₄⁺ in wells with the highest [NH₄⁺] shows that an autotrophic NO₂⁻ reduction pathway (anaerobic NH₄⁺ oxidation or nitrifier-denitrification) drove N attenuation closest to the contaminant plume. This direct empirical evidence that both autotrophic and heterotrophic biogeochemical processes drive N attenuation in contaminated aquifers demonstrates the power of multiple N isotopes to untangle N cycling in highly complex systems.

© 2016 Elsevier Ltd. All rights reserved.

1. Introduction

Global freshwater resources, 30% of which are held in sub-surface aquifers, are under pressure due to the combination of increased human demand and decreasing natural supply (Griebler and Avramov, 2015; Klove et al., 2014). Effective means of remediating (removing) groundwater contaminants are therefore needed as on-going pollution simultaneously diminishes the

supply of potable water. Groundwater management strategies are often limited by a poor understanding of the biogeochemical controls on contaminant cycling. Improving measurements of nitrogen's (N) fate and transport in groundwater is a priority due to both its ubiquity, and the 'cascade' of environmentally deleterious outcomes produced during transport due to its reactivity (Galloway et al., 2003). In natural systems, groundwater [N] is determined by residence time (Hinkle and Tesoriero, 2014). However, diffuse nitrate (NO₃⁻) inputs (excess soil fertilisation, animal excreta) and point ammonium (NH₄⁺) inputs (sewage, industrial effluent) overwhelm time-based constraints on N fate and transport. Turnover is complicated further in industrially contaminated sites, where multiple, asynchronous, contaminants (including salts, heavy metals, and hydrocarbons) can alter both the processes and rates of N transformations (Kleinsteuber et al., 2012; Ponsin et al., 2014).

* Corresponding author. Present address: Centre for Coastal Biogeochemistry, School of Environment, Science and Engineering, Southern Cross University, PO Box 157, Lismore, NSW 2480, Australia.

E-mail address: naomi.wells@scu.edu.au (N.S. Wells).

¹ Present address: IDAEA-CSIC Spanish National Research Council, Barcelona, Spain.

Attenuation of groundwater N (defined as the conversion of reactive N species to inert nitrogen gas (N_2)) is thought to be driven by denitrification, the step-wise reduction of NO_3^- to nitrous oxide (N_2O) and N_2 . Biological denitrification occurs under anaerobic conditions, using carbon (C) or sulphide minerals, as electron donors (Burgin and Hamilton, 2008; Rivett et al., 2008). Abiotic denitrification (chemodenitrification) that uses iron as an electron donor can occur, although its prevalence remains uncertain (Jones et al., 2015). The attenuation of NH_4^+ in groundwater therefore depends on the coupling of NH_4^+ oxidation (nitrification: autotrophic conversion of ammonia (NH_3) to nitrite (NO_2^-) and then NO_3^- under aerobic conditions) with denitrification (Izbicki, 2014). This limits N attenuation to the plume fringe, as anaerobic conditions within the plume inhibit nitrification while oxygen (O_2) outside of the plume inhibits denitrification (Meckenstock et al., 2015). Yet evidence for the importance of processes such as anaerobic NH_4^+ oxidation (anammox: autotrophic conversion of NH_4^+ and NO_2^- to N_2 (Sonthiphand et al., 2014)), co-denitrification (conversion of NO_2^- and organic N to $N_2O + N_2$ (Selbie et al., 2015)), and nitrifier-denitrification (reduction of NO_2^- to $N_2O + N_2$ by autotrophic nitrifying bacteria (Kool et al., 2010)) challenge the assumption that NH_4^+ attenuation is controlled by coupled nitrification-denitrification. The different energetic controls on these attenuation pathways make identifying their role in N turnover fundamental to the development of effective remediation schemes.

However, accurately measuring the importance of these pathways in contaminated systems is difficult. Modelling N losses from redox chemistry is complicated by the fact that N transformations occur in micro-scale 'hot spots' that are easily missed in such regional-scale sampling campaigns (Meckenstock et al., 2015; Rivett et al., 2008). Stoichiometric approaches can be used to

estimate N attenuation rates and/or source mixing (Koh et al., 2010; Murgulet and Tick, 2013), but cannot be used in many contaminated groundwater sites when multiple sources of multiple chemical contaminants violate assumptions of mass conservation. Injecting ^{15}N labels, a typically robust tool for measuring N attenuation (Kellogg et al., 2005), is also not viable in many contaminated sites as it relies on the presence of a conservative tracer.

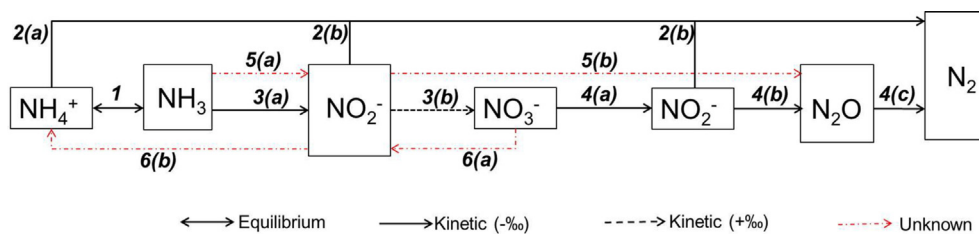
Advances in analysing the natural abundance composition of N species therefore create a potentially unique opportunity to assess N attenuation in contaminated groundwater (Hatzinger et al., 2013). This approach is based on the knowledge that the preferential use of heavy v. light isotopes during microbial reactions creates predictable Rayleigh-based patterns in the residual substrate pool: the ratio between the measured and initial substrate concentration (C/C_0) is related to the ratio between its measured and initial isotopic composition (R/R_0) by the reaction-specific fractionation factor (α) (Eq. (1)).

$$\frac{R}{R_0} = \left(\frac{C}{C_0}\right)^{\alpha-1} \quad (1)$$

Isotope values are reported in $\delta\text{‰}$, where the relative concentration is normalised to a standard; α values are reported as enrichment factors (ϵ ; $\epsilon = (\alpha - 1) \times 1000$). ϵ values are known for a growing number of N processes (Table 1): generally microbial preference for light isotopes causes the $\delta^{15}N$ of the residual substrate to increase as the reaction progresses ($\epsilon = -\text{‰}$), although some reactions cause inverse fractionation ($\epsilon = +\text{‰}$). As physical [N] changes (dilution or sorption) do not affect $\delta^{15}N$ composition, $\delta^{15}N$ patterns over time/distance can be used distinguish biological turnover from transport (Fenech et al., 2012).

Table 1

Overview of the microbial processes potentially affecting N fate in NH_4^+ contaminated aquifers. The N isotopic fractionation factors ($^{15}\epsilon$) for each step of each pathway are listed in table. (1) pH determines the chemical equilibrium between NH_4^+ and NH_3 , across which $^{15}\epsilon_{eq}$ is constant. (2) Under anaerobic conditions, NH_4^+ ($^{15}\epsilon_{amx,NH_4}$) can be coupled with NO_2^- ($^{15}\epsilon_{amx,NO_2}$) to create N_2 by anammox bacteria and archaea. (3) Under aerobic conditions, NH_3 is oxidised to NO_2^- ($^{15}\epsilon_{amo,NH_3}$) and then NO_3^- ($^{15}\epsilon_{amo,NO_2}$). (4) Denitrification sequentially reduces NO_3^- to NO_2^- ($^{15}\epsilon_{denit,NO_3}$), N_2O ($^{15}\epsilon_{denit,NO_2}$), and N_2 ($^{15}\epsilon_{denit,N_2O}$) under anaerobic conditions by using C as an electron donor. Denitrification driven by mineral oxidation (chemodenitrification) is also possible. (5) NH_3 oxidation can progress to N_2O production under low O_2 conditions, bypassing production and reduction of NO_3^- (6), and DNRA can occur under electron donor rich, low O_2 conditions, both with unknown effects on the isotopic composition of NH_3 , NO_3^- or NO_2^- .



ID	Process	Fractionation factor(s)	References
1	Chemical equilibrium	$^{15}\epsilon_{eq} = 20\text{‰}$	Casciotti et al., 2003
2	Anammox	(a) $^{15}\epsilon_{amx,NH_4} = -27 \pm 3\text{‰}$ (b) $^{15}\epsilon_{amx,NO_2} = -16 \pm 5\text{‰}$	(a,b) Brunner et al., 2013
3	Ammonia oxidation	(a) $^{15}\epsilon_{amo,NH_3} = -14 \rightarrow -38\text{‰}$ (b) $^{15}\epsilon_{amo,NO_2} = +12.8\text{‰}$	(a) Casciotti et al., 2003 (b) Casciotti 2009
4	Denitrification/chemodenitrification ^a	(a) $^{15}\epsilon_{denit,NO_3} = -3 \rightarrow -30\text{‰}$ (b) $^{15}\epsilon_{denit,NO_2} = -5 \rightarrow -25\text{‰}$ (c) $^{15}\epsilon_{denit,N_2O} = -31 \rightarrow -25\text{‰}$	(a) Granger et al., 2008, Kritee et al., 2012, Sebilo et al., 2003, Jones et al., 2015 ^a (b) Bryan et al., 1983, Casciotti et al., 2002 (c) Sutka et al., 2003, 2004
5	Nitrifier-denitrification ^b	(a) $^{15}\epsilon_{n-d,NH_3} = ?$ (b) $^{15}\epsilon_{n-d,NO_2} = ?$	
6	DRNA ^c	(a) $^{15}\epsilon_{DRNA,NO_3} = ?$ (b) $^{15}\epsilon_{DRNA,NO_2} = ?$	

^a Chemodenitrification causes comparable N isotope fractionation (Jones et al., 2015).

^b Fractionation factors for nitrifier-denitrification have not been directly measured, but may reasonable be expected to be comparable to those for the NH_3 oxidation for step (a) as the same enzymes and microbial populations are involved (Kool et al., 2010; Colliver and Stephenson, 2000).

^c There are no direct measurements of fractionation factors for DNRA, but anomalous relationships between $\delta^{15}N-NO_3^-$ and $\delta^{18}O-NO_3^-$ have been reported in regions where DNRA is known to occur (Dhondt et al., 2003).

Knowledge that NO_3^- reduction enriches $\delta^{15}\text{N}$ and $\delta^{18}\text{O}$ of the residual pool at a 1:1 \rightarrow 1:2 ratio (Xue et al., 2009) makes NO_3^- dual isotopes a useful indicator of denitrification in a range of freshwater environments (Clague et al., 2015; Fang et al., 2015; Wells et al., 2016). However, quantifying N attenuation using NO_3^- dual isotopes is limited due to, 1) mixing of isotopically distinct source pools can mask the fractionation patterns created by partial denitrification, and, 2) focusing solely on NO_3^- isotope dynamics ignores the possible role of non-denitrification based attenuation pathways (Fenech et al., 2012; Xue et al., 2009).

Improved information on 'alternative' N transformations (Table 1) and analytical techniques (McIlvin and Casciotti, 2011) create possibilities for overcoming these limitations. We hypothesised that measuring isotope patterns within multiple N species ($\delta^{15}\text{N}-\text{NO}_3^-$, $\delta^{18}\text{O}-\text{NO}_3^-$, $\delta^{15}\text{N}-\text{NO}_2^-$, and $\delta^{15}\text{N}-\text{NH}_4^+$) would enable N attenuation pathways across contaminated sites to be quantified, independent of the quality of prior information on N sources and flow paths available. To test this, we developed a multi-isotope analytical framework to constrain both the occurrence and drivers of attenuation within a complex NH_4^+ contaminated groundwater system.

2. Materials & methods

2.1. Site description

The study was carried out at a >100 year old industrial area in

western Belgium that is underlain by an unconfined shallow sand aquifer (local) and deeper, partially unconfined, chalk aquifer (regional) along the northern flank of a syncline shaped basin (Fig. 1). The sand aquifer is 5–15 m thick, and the chalk aquifer increases from 15 to more than 100 m thickness from north to south. The chalk formation outcrops in the north, where recharge occurs, then dips below the sand aquifer and becomes confined in the south. An impervious marl layer impedes groundwater inflow from the underlying fractured limestone aquifer, and an impervious clayey layer (1–10 m thick) restricts groundwater exchanges between the sand and chalk aquifers (Marliere, 1977). Groundwater flows N–S below the megasite in both aquifers, and from east to west in the central basin of the chalk (Fig. 1). Although pre-contamination data for the megasite is sparse, comparison with nearby aquifers with similar geology indicates that both have calcium-bicarbonate type water (Service Publique de Wallonie, 2006).

Water quality is monitored in five zones in the chalk aquifer (North, Waste, West, downgradient (DG), and far downgradient (Far)) and two in the smaller sand aquifer (Waste, DG). The North, Waste, and West zone underlay the industrial site, with DG and Far zones downgradient. Well depths within these zones increased along the N–S flow path (sand: 7–11 m (Waste) to 9–13 m (DG); chalk: 11–18 m (North), 13–22 m (West), 26–36 m (Waste), 28–38 m (DG), 94–104 m [Far]). Screen lengths vary over the site, in part because wells within the contaminant zone were set to best capture the contaminant plume based on soil and groundwater

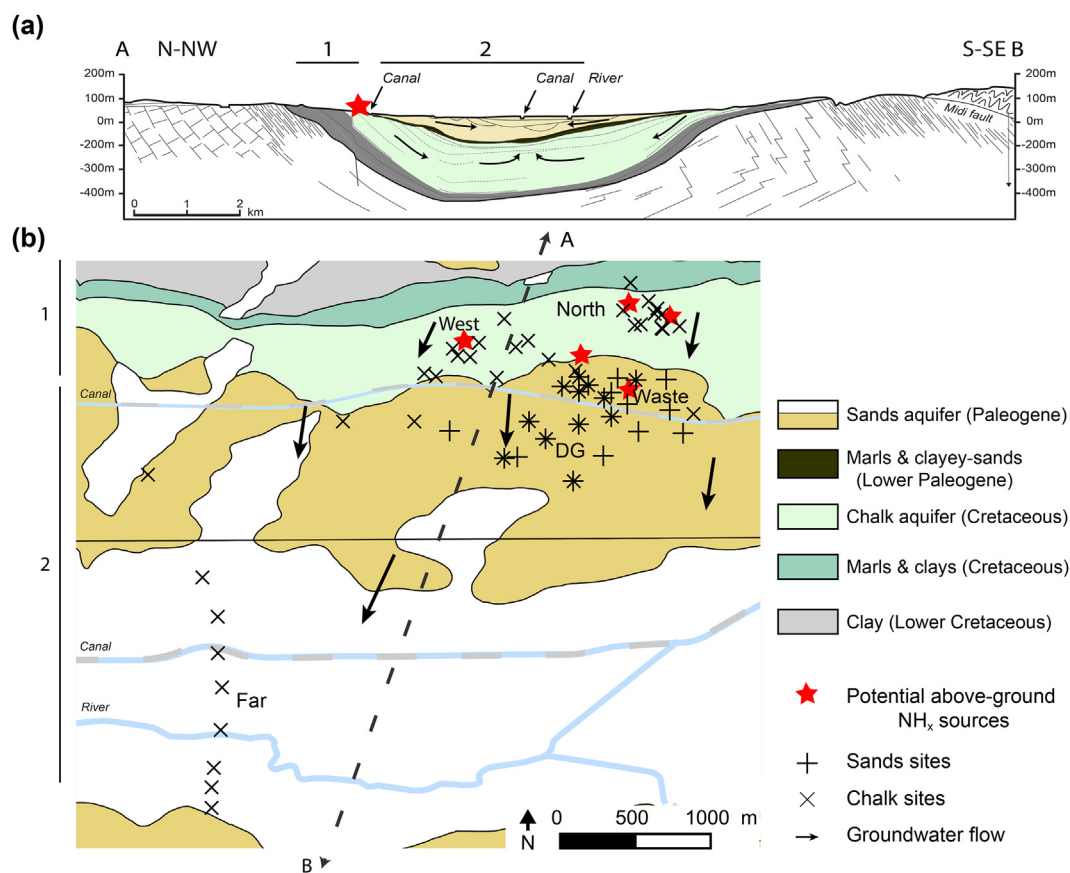


Fig. 1. (a) The groundwater system underlying an intensive industrial area (red star) is comprised of chalk and sand aquifers that are separated by an impermeable layer. One canal, which is hydrologically isolated from the groundwater, cuts through the sampled areas (1, 2). (b) Groundwater was collected from wells in the chalk aquifer in the unconfined North region and adjacent West confined area (1) and downgradient from the contaminant zone (Far, DG; 2). Wells in the overlying, unconfined sand aquifer were sampled in the Waste and DG zones. Arrows indicate groundwater flow direction. The cross-section (a) corresponds to the solid line along the N-NW and S-SE axes in (b). (Modified from Marliere (1977)). (For interpretation of the references to colour in this figure legend, the reader is referred to the web version of this article.)

screening data (Suppl. Mat.). Contaminants are concentrated in the Waste zone of both aquifers, plus the North zone of the chalk aquifer. However, the site's long industrial history and poor records availability, combined with the presence of multiple contaminants (including toxic levels of organics, metals, salts, nutrients [S. Brouyère, unpublished data]), have previously made accurate assessment of groundwater N sources and sinks difficult. Potential N sources to the groundwater include: the West zone surface settling ponds, coking effluent in the NE, and fertiliser production in the North zone (Fig. 1).

2.2. Sample collection

Groundwater was sampled from 24 locations within the sand aquifer (12 Waste and 12 DG) and 52 within the chalk aquifer (12 North, 9 Waste, 11 West, 11 DG, and 9 Far) in August 2013. Water was pumped up at $<10 \text{ l min}^{-1}$ and passed through a $0.45 \mu\text{m}$ filter. Samples were collected once conductivity and water temperature (T) stabilised. Aliquots (100 ml) were collected for ion, carbonate (HCO_3^-) and total organic C (TOC) analysis. For N analyses, water was passed through an additional $0.22 \mu\text{m}$ Sterivex filters (Millipore) and two 100 ml Nalgene bottles filled. Replicates for NH_4^+ analysis were stabilised by adding 1 ml of 6 M HCl (i.e., NH_4^+ values reported here represent $\text{NH}_4^+ + \text{NH}_3$). Samples were kept at 4°C for <2 weeks and then frozen until analysis. Conductivity, T, pH, redox potential (Eh) and dissolved oxygen (DO) were measured *in-situ* using a multi-parameter probe (YSI 556 MPS).

2.3. Chemical analyses

Cations (Ca^{2+} , Mg^{2+} , Na^+ and K^+) and anions (Cl^- , SO_4^{2-} , Br^- and NO_3^-) were measured via ion chromatography (Metrohm MCS – 850 Professional IC AnCat) at the University of Liège (ArGenCo Dept.). A UV–vis (Specord200, analytik Jena) was used to measure $[\text{NO}_2^-]$ and $[\text{NH}_4^+]$. Nitrite was measured prior to freezing using the sulfanilimide method (detection limit = $0.001 \text{ mg NO}_2^- \text{ N l}^{-1}$), with absorbance read at 410 nm. Nessler's reagent was used to measure $[\text{NH}_4^+]$ in acidified samples, with absorbance read at 425 nm.

Isotope data is reported in $\delta\text{‰}$ relative to international standards (AIR for N; VSMOW for O and H). Water isotope ($\delta^{18}\text{O}$ and δD of H_2O) composition was measured on a liquid water isotope analyser (Los Gatos). Analytical precision was $<0.15\text{‰}$ ($\delta^{18}\text{O}$) and $<0.5\text{‰}$ (δD) for all samples (based on $5\times$ replicate analysis of samples, with the first two discarded). Samples were normalised to the VSMOW scale using replicate ($20\times$) analysis of internal standards calibrated to VSMOW and SLAP certified reference materials. Nitrite isotopes were measured by adding azide to samples to produce N_2O (Casciotti et al., 2007; McIlvin and Altabet, 2005). $\delta^{18}\text{O}-\text{NO}_2^-$ data were discarded due to equilibration with ambient $\text{O}-\text{H}_2\text{O}$. $\delta^{15}\text{N}-\text{NH}_4^+$ was measured in the acidified aliquots using BrO^- to oxidise NH_x to NO_2^- , which was then reacted with azide to produce N_2O (Zhang et al., 2007). Nitrate was converted into N_2O using the denitrifier method (McIlvin and Casciotti, 2011). The N_2O produced from each reaction was then measured on a DeltaPlus IR-MS fitted with a gas bench (Dept. of Catchment Hydrology, UFZ). All samples were prepared in duplicate, in batches containing water blanks and the relevant international (NH_4^+ : USGS-24 and USGS-25; NO_3^- : USGS-32, USGS-34, USGS-35) and internal lab standards ($(\text{NH}_4)_2\text{SO}_4$: $\delta^{15}\text{N} = -0.3\text{‰}$; KNO_3 : $\delta^{15}\text{N} = 1.5\text{‰}$ and $\delta^{18}\text{O} = 22.8\text{‰}$). There are no certified NO_2^- isotope standards, so values were calibrated using two internal standards (NaNO_2 : $\delta^{15}\text{N}$ of -18.4‰ ; KNO_2 : $\delta^{15}\text{N}$ of -13.7‰) and two cross-referenced standard salts from Helmholtz Zentrum Munich (Zh-1: $\delta^{15}\text{N}$ of -16.4‰ ; MAA1: $\delta^{15}\text{N}$ of -60.6‰) that had been measured as solids using EA-IR-MS. Method precision for $\delta^{15}\text{N}$ of NH_4^+ and NO_2^- was $\pm 0.3\text{‰}$; NO_3^-

method precision was $\pm 0.4\text{‰}$ and $\pm 0.6\text{‰}$ for $\delta^{15}\text{N}$ and $\delta^{18}\text{O}$, respectively.

2.4. Data analysis

Data were checked for normality. Non-parametric Mann-Whitney U and Kruskal-Wallis tests were used to test for differences between the chalk and sand aquifers and between the zones within each aquifer. The first step to identifying contaminant source zones was to establish the relationships between chemical constituents within each aquifer using Spearman rank-order correlation. Principle component analyses (PCA) were then conducted to identify different contaminant sources within both the sand and the chalk aquifer. In order to keep this indicator independent from the N isotope data, two components were extracted based on water chemistry parameters (Cl^- , Na^+ , Mg^{2+} , conductivity, pH, HCO_3^- , Mn^{2+} , $\delta\text{D}-\text{H}_2\text{O}$, and $\delta^{18}\text{O}-\text{H}_2\text{O}$). Forward and backward variable exclusion was used to determine best model fit, and covariant and insignificant factors were excluded.

Linear regressions performed on H_2O (δD and $\delta^{18}\text{O}$) and NO_3^- ($\delta^{18}\text{O}$ and $\delta^{15}\text{N}$) dual isotope pairs were evaluated for goodness of fit (r^2) and 95% confidence intervals (CIs). The effects of biological processes on $\delta^{15}\text{N}$ of each species was estimated using the enrichment factors listed in Table 1 using the simplified Rayleigh equations from Mariotti et al. (1981), Casciotti (2009), and Casciotti et al. (2003). The $\delta^{15}\text{N}$ composition of DIN ($\text{NH}_4^+ - \text{N} + \text{NO}_2^- - \text{N} + \text{NO}_3^- - \text{N}$) in each well was calculated for each sampling location based on the concentration-weighted mean of the measured $\delta^{15}\text{N}-\text{NH}_4^+$, $\delta^{15}\text{N}-\text{NO}_2^-$, and $\delta^{15}\text{N}-\text{NO}_3^-$. Data analyses were carried out using SPSS (ver. 21) and SigmaPlot (ver. 13). Significance is defined as $p < 0.05$, and, unless otherwise specified, all values are reported as mean \pm standard deviation.

3. Results

3.1. Water chemistry

Water isotope values ranged from -7‰ to -5‰ ($\delta^{18}\text{O}-\text{H}_2\text{O}$) and -50‰ to -20‰ ($\delta\text{D}-\text{H}_2\text{O}$), moving along a slope of 3.7 (95% CI: 3, 6) in the sand aquifer and 5.7 (95% CI: 5, 9) in the chalk aquifer. Both $\delta^{18}\text{O}-\text{H}_2\text{O}$ and $\delta\text{D}-\text{H}_2\text{O}$ were lowest in the unconfined North zone of the chalk aquifer, and $\delta^{18}\text{O}-\text{H}_2\text{O}$ values were highest ($p < 0.05$) in the Waste zone of the chalk aquifer (Fig. 2a). Waste zones in both aquifers were more reducing, and the North zone the most oxidising ($p < 0.01$; Table 2). Groundwater pH was <6 in five wells within the chalk aquifer and two within the sand aquifer (Table 2). One well within the North zone of the chalk aquifer had $\text{pH} < 3$. Low-pH wells were located within the Waste (sand and chalk), plus one each in the DG and North (chalk) zones.

The Waste zones contained the highest concentrations of both redox sensitive (NH_4^+ , NO_3^- , SO_4^{2-} , Mn^{2+}) and non-reactive (Na^+ , K^+ , Cl^-) ions. However, inter-well variability was high (Table 2, Fig. 3). PCA identified three distinct chemical compositions. In each aquifer, the majority of wells clumped in one group, with two distinct 'outlier' groups (Fig. 2). Wells within the outlier groups were located up-gradient (Waste in sand; West, North, and Waste in chalk) and had above average concentrations of all measured chemical constituents. In the chalk aquifer, one outlier group (C1) was characterised by high $[\text{HCO}_3^-]$ (1400 mg l^{-1}) and the other (C2) by high $[\text{Mg}^{2+}]$ (180 mg l^{-1}) and low pH (4.8). Similarly, in the sand aquifer group one outlier group (S1) was characterised by high $[\text{HCO}_3^-]$ (3400 mg l^{-1}) and the other (S2) by high $[\text{Mg}^{2+}]$ (36 mg l^{-1}) and low pH (5.4). In both aquifers, wells within the Far and DG zones were located farthest from the outlier groups, both on the PC axes and geographically (Figs. 2 and 3).

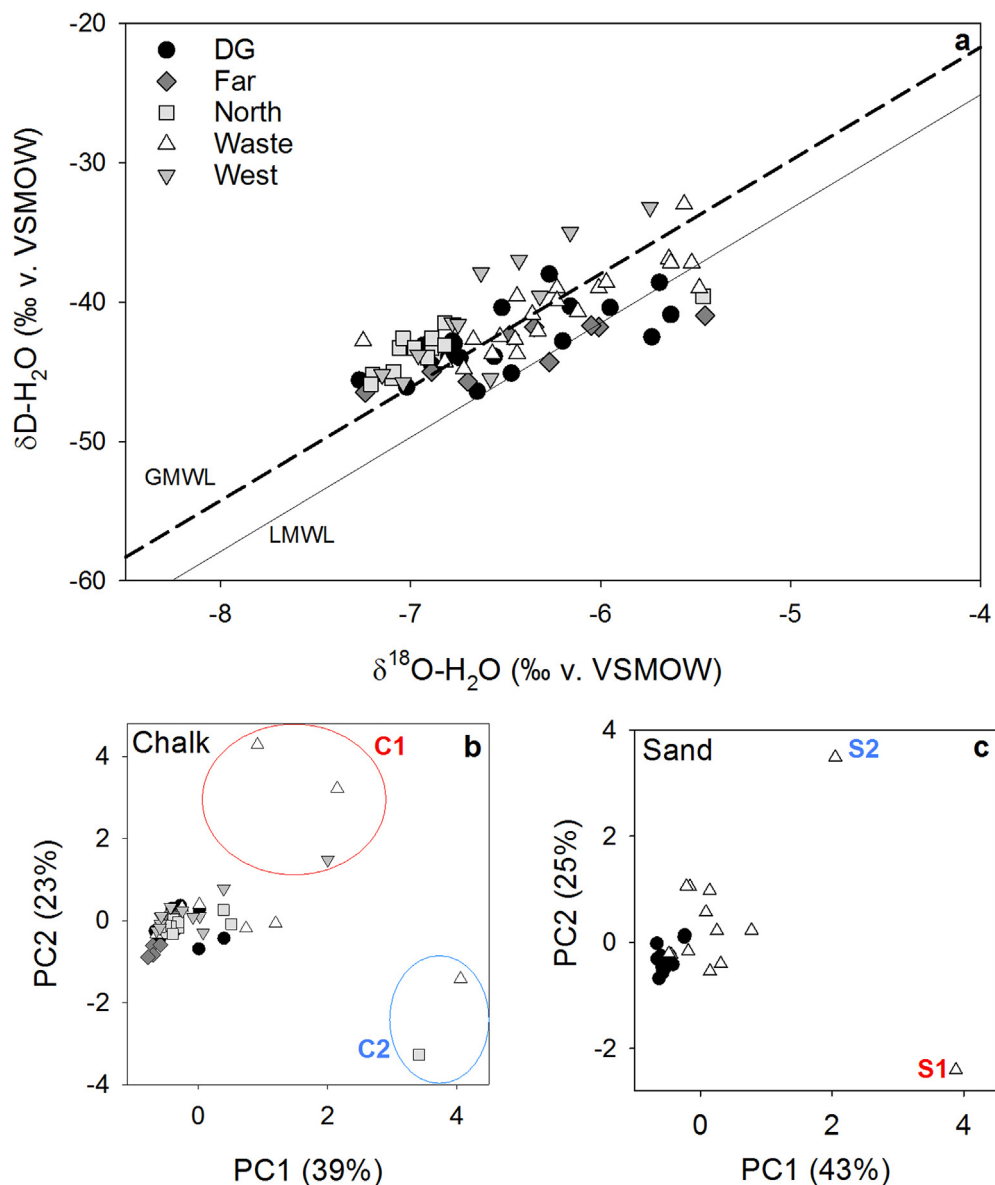


Fig. 2. The isotopic (a) and chemical (b,c) composition of groundwater in a shallow sand aquifer ($n = 24$) and the deeper, confined chalk aquifer ($n = 40$) underlying an industrial site in eastern Belgium. In (b) and (c) the PCA of groundwater chemistry are projected onto axes for the first two PCs, and percentage of variance explained noted on their respective axes. Outlier values are labelled S1 (red) and S2 (blue) in sand, C1 (red) and C2 (blue) in chalk. Axes in (b) describe 58% (x) and 29% (y) of variance, and were primarily driven by HCO_3^- , Mg^{2+} , and K^+ . Axes in (c) describe 43% (x; primarily driven by K^+ , Na^+ , and HCO_3^-) and 25% (y; primarily driven by Cl^- and Mg^{2+}) of variance. (For interpretation of the references to colour in this figure legend, the reader is referred to the web version of this article.)

3.2. Nitrogen dynamics

[DIN] ranged from <1 (Far) to 1300 (Waste) mg N l^{-1} in the chalk aquifer and from <1 (DG) to 1900 (Waste) mg N l^{-1} in the sand aquifer. Maximal values for both occurred in the Waste zones. Chalk aquifer $\delta^{15}\text{N-DIN}$ values ranged from -14‰ to $+31\text{‰}$ within the Waste and West zones, but generally increased over the flow path ($p < 0.05$) (Fig. 6). In the chalk aquifer, but not the sand, there was an inverse relationship between [DIN] and $\delta^{15}\text{N-DIN}$ ($p < 0.01$). Redox potential negatively correlated with [DIN] in the sand aquifer ($p < 0.05$), while chalk aquifer [DIN] correlated with neither DO nor redox potential.

3.2.1. Ammonium

Ammonium dominated the DIN pool in most wells, with chalk aquifer concentrations from 0 to 1000 mg N l^{-1} (6.5 ± 11 mg N l^{-1} in

Far to 240 ± 300 mg N l^{-1} in Waste to) and sand aquifer concentrations from <1 to 920 mg N l^{-1} (4 ± 9 mg N l^{-1} in DG to 280 ± 300 mg N l^{-1} in Waste). In both aquifers, $[\text{NH}_4^+]$ was highest in the northern Waste zone (Fig. 3a). $\delta^{15}\text{N-NH}_4^+$ values were highly variable between wells within each sampling zone, but tended to be more negative within the Waste zones (Fig. 4). Concentrations positively correlated with Mg^{2+} , Cl^- , SO_4^{2-} , K^+ , Na^+ , and conductivity, and negatively correlated with redox potential ($p < 0.05$). In the sand aquifer, $[\text{NH}_4^+]$ negatively correlated with $\delta^{15}\text{N-NH}_4^+$ ($p < 0.05$; Fig. 4). Conductivity and $\delta^{15}\text{N-NH}_4^+$ negatively correlated in both aquifers ($p < 0.01$). Wells within the outlier PCA groups corresponded with some of the maximal $[\text{NH}_4^+]$ and minimal $\delta^{15}\text{N-NH}_4^+$ values (Fig. 4).

3.2.2. Nitrite

Nitrite was the smallest proportion of DIN. Concentrations

Table 2
Distribution of chemical constituents across a shallow sand aquifer and a deep chalk aquifer that underlie an industrial site in eastern Belgium. Samples were collected from zones directly below known contaminant sources (North, Waste, and West) and farther downgradient (DG, Far). Due to the extreme variability of concentrations within the contaminant sources zones, values are expressed here as minimum – maximum (mean). Letters indicate significant difference ($p < 0.05$) between zones; * indicates significant difference between aquifers.

Zone	Chalk							Sand													
	TOC mg C l ⁻¹	Redox* mV	pH	Conductivity µS cm ⁻¹	HCO ₃ ⁻ Mg l ⁻¹	Na ⁺	K ⁺	Mg ²⁺	SO ₄ ²⁻	Cl ⁻	TOC* mg C l ⁻¹	Redox mV	pH	Conductivity µS cm ⁻¹	HCO ₃ ⁻ mg l ⁻¹	Na ⁺	K ⁺ *	Mg ²⁺	SO ₄ ²⁻	Cl ⁻	
North	1.1–36 (11)	-98–250 (110)a	2.9	1000–9400 (2800) a	34–520 (320)	6.3–390 (48)	2.6–43 (9.5)	5.5–140 (30) a	130 (1300)	4.5–44 (24) b	–	–	–	–	–	–	–	–	–	–	–
Waste	2.1–170 (38) a	-430 – -14 (-210) b	6.4	510–9900 (4900) a,b	170 (710) a	2.6–520 (150)	4.7–52 (24)	4.5–210 (39)	23–1800 (610)	20–3400 (780) a	4.0–900 (150) a	4.7	990–14,000 (5300) a	15 (550)	9.1–2600 (300) a	9.5–950 (210) a	3.8	31–2400 (1200) a	8.5–3500 (630) a	–	–
West	1.7–48 (8.4)	-270–59 (-120)	6.7	740–10,000 (2800) a,b	130–500 (330)	7.8 (160)	4.4–140 (38) a	4.0–18 (9.5)	88–1600 (710)	24–2300 (280)	–	–	–	–	–	–	–	–	–	–	–
DG	1.2–8.0 (3.6)	-150–140 (-56)	3.9	470–3300 (1800) b	7.0–480 (260)	4.3–250 (69)	7.8–25 (15)	4.4–32 (13)	17–970 (370)	13–980 (220)	3.4–63 (17)	6.1	160–2300 (930)	5.9–480 (280)	1.8–130 (22)	2.9–29 (10)	1.6	21–780 (210)	3.9–170 (56)	–	–
Far	n.d.	-140 (-83)	7.3	320–1700 (970) b	130–720 (150)	16–78 (51)	4.0–14 (7.8) b	3.2–13 (8.4)	19–510 (220)	46–98 (74)	–	–	–	–	–	–	–	–	–	–	–

ranged from 0 to 0.6 mg N l⁻¹ in the chalk aquifer and from 0 to 0.8 mg N l⁻¹ in the sand (Table 3). The highest concentrations occurred in the Waste zones (Table 3). Values of $\delta^{15}\text{N}-\text{NO}_2^-$ varied from -42‰ to +37‰, though wells in the Far zone displayed the narrowest, consistently negative, range (Table 3). Within the sand aquifer, $[\text{NO}_2^-]$ positively correlated with $[\text{NH}_4^+]$ and conductivity ($p < 0.001$). There was no relationship between $[\text{NO}_2^-]$ and $[\text{NH}_4^+]$ in the chalk aquifer, although $[\text{NO}_2^-]$ and $[\text{DIN}]$ correlated ($p < 0.01$). In both aquifers, $[\text{NO}_2^-]$ positively correlated with $\delta^{15}\text{N}-\text{NO}_2^-$ composition ($p < 0.01$).

3.2.3. Nitrate

$[\text{NO}_3^-]$ ranged from 0 to 360 mg N l⁻¹ (from 3 ± 5 mg N l⁻¹ (Far) to 60 ± 100 mg N l⁻¹ (Waste)) in the chalk aquifer, and from 0 to 1000 mg N l⁻¹ in the sand (Fig. 5). $[\text{NO}_3^-]$ contributed the least to $[\text{DIN}]$ in the Waste and DG zones ($9 \pm 10\%$ and $20 \pm 30\%$, respectively), in contrast to the $50 \pm 40\%$ and $70 \pm 40\%$ it contributed in the West and North zones, respectively. The Waste (chalk and sand) and North zones contained both the highest $[\text{NO}_3^-]$ and numerous wells with $[\text{NO}_3^-]$ of ~0 (Fig. 5a,c). Wells in S1 and S2 had negligible $[\text{NO}_3^-]$ (Fig. 5c), while $[\text{NO}_3^-]$ ranged from high to low over the flow gradient in wells within C1 and C2 (Fig. 5a). In both aquifers, $[\text{NO}_3^-]$ and $[\text{NH}_4^+]$ positively correlated (sand: $p < 0.01$; chalk: $p < 0.001$) (Fig. 3). $[\text{NO}_3^-]$ negatively correlated with $\delta^{15}\text{N}-\text{NO}_3^-$ ($p < 0.05$), but not $\delta^{18}\text{O}-\text{NO}_3^-$, in both aquifers (Fig. 5a,c). In both aquifers $\delta^{18}\text{O}-\text{NO}_3^-$ and $\delta^{15}\text{N}-\text{NO}_3^-$ increased over the flow path ($p < 0.01$). The overall relationship between $\delta^{18}\text{O}-\text{NO}_3^-$ and $\delta^{15}\text{N}-\text{NO}_3^-$ was not significant (Fig. 5b,d). In the chalk aquifer, $[\text{NO}_3^-]$ correlated negatively with $\delta^{15}\text{N}-\text{NO}_2^-$; in the sand aquifer, $\delta^{15}\text{N}-\text{NO}_3^-$ positively correlated with $\delta^{15}\text{N}-\text{NH}_4^+$ ($p < 0.01$).

4. Discussion

4.1. Nitrogen sources

Groundwater in infiltration zones (the sand aquifer and the North zone of the chalk aquifer) exhibited slightly different H₂O isotopic composition than that farther downgradient in the confined portions of the chalk aquifer. The lack of systematic shifts in the H₂O isotopic composition over the flow path suggest that these differences are driven by the fact that the local rainfall patterns that affect the infiltration zone become homogenized during transport through the confined aquifer, and not the influx of an additional water source downgradient. This supports previous findings that, 1) the downgradient area of the chalk aquifer is completely confined, and, 2) recharge for both aquifers originates in the same geographic area (Izbicki, 2014). There was likewise no evidence of infiltration of water with a unique ionic composition in any of the sampled zone, and water chemistry within both aquifers progressively shifted away from that in the wells with the most extreme contaminant loads (Koh et al., 2010). This hydrologic setting makes it possible to analyse the N dynamics based on the assumption that activities around the up-gradient, unconfined area (North, West, Waste) provide the sole source of N inputs to either aquifer.

4.1.1. Ammonium

The multiple, spatially discontinuous, locations with extreme $[\text{NH}_4^+]$ (>600 ppm) across the megasite indicate the presence of multiple N sources (Fig. 2). This contrasts previous isotope-based investigations of NH_4^+ contaminated aquifers (Clark et al., 2008; Izbicki, 2014; Robertson et al., 2012). Previously, a single, continuously reacted, NH_4^+ plumes enabled the site-specific source composition (R_0 , subsequently referred to as $\delta^{15}\text{N}_0$) to be identified using Eq. (1), which stipulates that $\delta^{15}\text{N}_0$ is the point with the highest $[\text{NH}_4^+]$ and lowest $\delta^{15}\text{N}-\text{NH}_4^+$. The fairly weak relationship

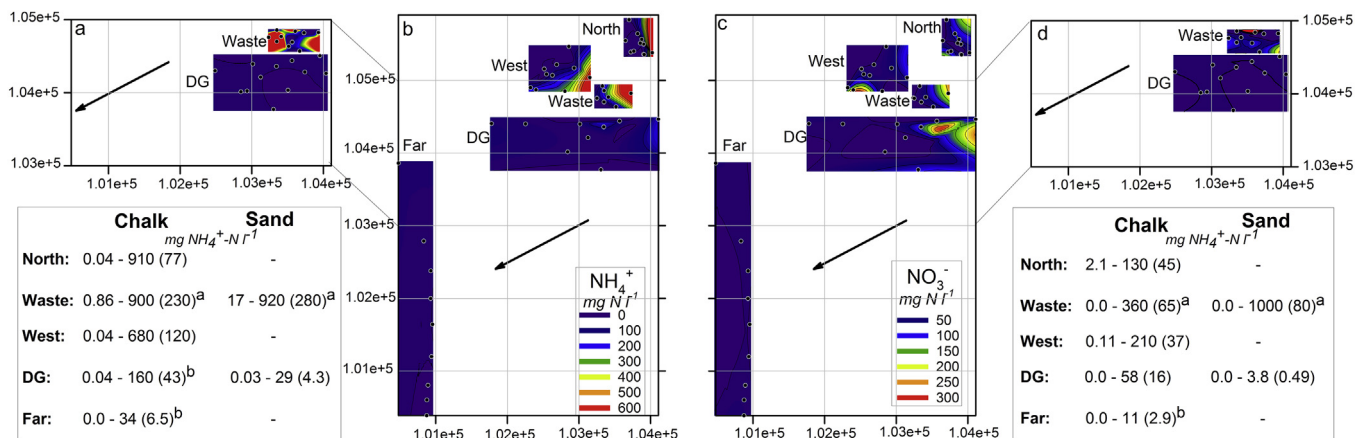


Fig. 3. Distribution of NH₄⁺ (a,b) and NO₃⁻ (c,d) across the chalk (b,c) and sand (a,d) aquifers underlying an industrial megasite. Groundwater samples were taken from the chalk aquifer across five zones, three directly below the industrial area (North, Waste, West) and two downgradient from it (DG and Far). The sand aquifer was sampled in Waste and DG zones. Non-linear kriging was used to interpolate between sampling locations (indicated by black circles). Minimum, maximum (and mean) values of the compounds in each zone are listed below the corresponding figure, with letters indicating significant difference (*p* < 0.05). Axes display arbitrary numbers that are 1:1 equivalent to UTM units, in accordance with site confidentiality agreements.

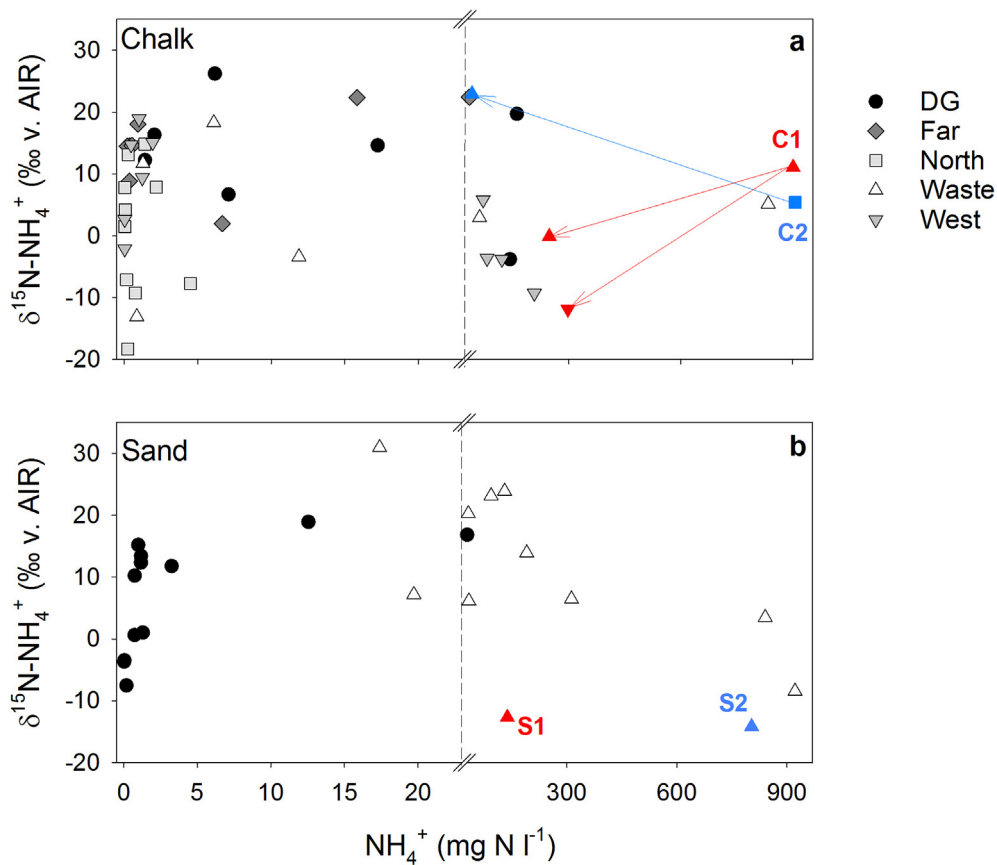


Fig. 4. Relationship between NH₄⁺ concentration and isotopic composition within the chalk (a) and sand (b) aquifers underlying an industrial site in eastern Belgium. Samples were collected from 70 locations directly under the site (light colours: North, Waste, West) and further downgradient (dark colours: DG, Far). Hypothesised contaminant source locations indicated with red (S1, C1) and blue (S2, C2) symbols, with arrows between points indicating regional flow direction. Note change in x-axis scale after 25 mg N l⁻¹. (For interpretation of the references to colour in this figure legend, the reader is referred to the web version of this article.)

between [NH₄⁺] and δ¹⁵N–NH₄⁺ within the study area corroborates the picture of multiple N sources within both aquifers. An independent line of evidence was therefore needed to constrain the location and composition of N sources.

Multi-variate analysis of the non-N water chemistry highlighted two locations disproportionately affecting downgradient

chemistry: 1) a low pH, high conductivity, area in the northern Waste zone to the SE of the North zone (S2, C2), and, 2) a Mg²⁺ rich area in the western Waste zone (S1, C1). As expected based on the strong correlations between the species, these locations also encompassed the highest NH₄⁺ concentrations and most depleted δ¹⁵N–NH₄⁺ and δ¹⁵N–DIN values, making it reasonable to define

Table 3
The concentration and $\delta^{15}\text{N}$ composition of NO_2^- in five zones (North, Waste, West, DG, Far) across the chalk and sand aquifers underlying a contaminated industrial site. Nitrite was measured in a total of 65 wells in October 2013. Letters indicate within-aquifer differences ($p = 0.056$ in chalk; $p < 0.05$ in sand).

Zone	Chalk		Sand	
	NO_2^-	$\delta^{15}\text{N}-\text{NO}_2^-$	NO_2^-	$\delta^{15}\text{N}-\text{NO}_2^-$
	mg N l ⁻¹	‰ v. AIR	mg N l ⁻¹	‰ v. AIR
North	0.0017–0.47 (0.094) a	–18–15 (1.1)	–	–
Waste	0.0–0.24 (0.069)	–24–15 (–3.8)	0.0–0.80 (0.24) a	–14 – +37 (2.8)
West	0.0007–0.59 (0.10) a	–12–19 (3.3)	–	–
DG	0.0014–0.017 (0.0060)	–42–6.4 (–21)	0.0–0.030 (0.0069)	–41 – +11 (–11)
Far	0.0006–0.011 (0.0037)	–14 – –6.3 (–9.8)	–	–

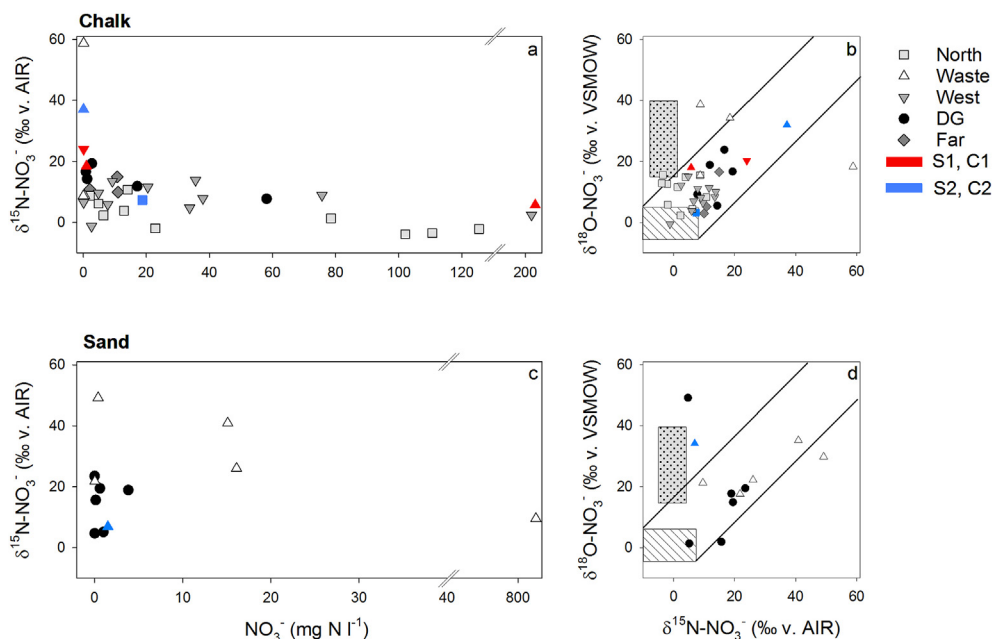


Fig. 5. Relationships between $[\text{NO}_3^-]$ and $\delta^{15}\text{N}-\text{NO}_3^-$ (a,c) and $\delta^{15}\text{N}-\text{NO}_3^-$ and $\delta^{18}\text{O}-\text{NO}_3^-$ (b,d) within the regional chalk (top) and local sand (bottom) aquifers underlying a historic industrial site. Chalk aquifer samples were collected from directly underneath the industrial area (dark: North ($n = 12$), Waste ($n = 9$), West ($n = 10$)) and farther down gradient from the contamination (light: DG ($n = 11$), Far ($n = 9$)). Sand aquifer samples were collected in the Waste ($n = 12$) and DG ($n = 12$) zones. Dashed rectangles in the dual isotope plots represent the expected NO_3^- composition based on measured $\delta^{15}\text{N}-\text{NH}_4^+$ and $\delta^{18}\text{O}-\text{H}_2\text{O}$ composition and the hatched rectangle covers the range expected for NO_3^- from fertilisers ($\delta^{18}\text{O} \sim 15\text{‰}$) and atmospheric deposition ($\delta^{18}\text{O}$: 20‰–50‰). Solid lines represent the 1:1 $\delta^{18}\text{O}:\delta^{15}\text{N}$ enrichment ratios expected for denitrification (Xue et al., 2009). Hypothesised N source locations are marked red (C1, S1) or blue (C2); NO_3^- was not detected in S2. (For interpretation of the references to colour in this figure legend, the reader is referred to the web version of this article.)

them as the effective $\delta^{15}\text{N}_0$ values (source plumes) for the aquifers. These differences in water chemistry between the identified NH_4^+ sources help to exclude the possibility of sampling design (variations in well types and screen depths) influencing the data.

The fact that the chemical composition and spatial location of these two contaminant groupings were the same in aquifers that are not hydrologically connected supports previous assumptions that pollution originates from industries above the unconfined northern region of the site. Specifically, the western contaminant source (S1, C1) coincides with the chemical settling ponds and the eastern (S2, C2) with the former coking plant. The -10‰ $\delta^{15}\text{N}_0$ values are lower than the $\sim +4\text{‰}$ values previously reported for sewage (Goody et al., 2014; Hinkle et al., 2008; Hood et al., 2014) and coking effluent (Karthic et al., 2013), but similar to those reported for chemical NH_4^+ fertilisers (Xue et al., 2009). However, there is not enough information on variations in $\delta^{15}\text{N}$ between NH_4^+ sources to use these values for conclusive source identification. For the purposes of developing an isotopic model of N sources and sinks, it is sufficient to say that two NH_4^+ sources with similar isotopic composition exist within the chalk ($-10\text{‰} - +5\text{‰}$) and sand ($-14\text{‰} - -10\text{‰}$) aquifers.

4.1.2. Nitrate

High $[\text{NO}_3^-]$ within the contaminant zone, combined with knowledge of crop and fertiliser production in the North zone, mean that the possibility of a direct NO_3^- source must also be considered. Nitrate isotopes can be used to distinguish fertiliser inputs from *in-situ* nitrification: $\delta^{18}\text{O}$ of fertiliser NO_3^- has values from $+15\text{‰}$ to $+25\text{‰}$ and $\delta^{15}\text{N}$ values of -0‰ (Xue et al., 2009), while nitrification would here produce NO_3^- with $\delta^{15}\text{N}$ values between -20‰ and $+5\text{‰}$ (as per Rayleigh fractionation, Table 1) and $\delta^{18}\text{O}$ values of $3.3 \pm 0.3\text{‰}$ (2:1 mixing of $\text{O}-\text{H}_2\text{O}$ and $\text{O}-\text{O}_2$ ($+23.5\text{‰}$), plus $\sim 5\text{‰}$ uncertainty from possible kinetic and equilibrium fractionation during O incorporation (Buchwald and Casciotti, 2013)). Subsequent denitrification would cause both $\delta^{18}\text{O}$ and $\delta^{15}\text{N}$ to increase in parallel (Fig. 5). As six wells had $\delta^{18}\text{O}-\text{NO}_3^-$ values higher than could be explained by nitrification + denitrification it is possible that NO_3^- fertiliser affects the groundwater N pool (Fig. 5). Critically, the NO_3^- loads within these wells were relatively low ($< 5 \text{ mg N l}^{-1}$). In contrast, wells with the highest $[\text{NO}_3^-]$ had $\delta^{15}\text{N}$ and $\delta^{18}\text{O}$ values within the predicted nitrification range. *In-situ* NO_3^- production is also supported by the isotope dynamics between NH_4^+ and NO_3^- : $[\text{NO}_3^-]$ was

<1 mg N l⁻¹ in S1 and S2, which had a relatively homogeneous $\delta^{15}\text{N-NH}_4^+$ composition, while the highest $\delta^{15}\text{N-NH}_4^+$ ‘source’ value (C1) occurred in the only well where NO_3^- comprised a significant proportion of the DIN pool. The >100-fold concentration difference between the identified *in-situ* NH_4^+ sources and the possible NO_3^- fertiliser source makes it reasonable to conclude that fertiliser would have a minimal effect on downgradient N pools. Although finer scale measurements of these areas are suggested in order to fully quantify the factors driving variations in $\delta^{15}\text{N}_0$, the broad constraints on the composition and location of the N pollution sources here were sufficient to enable the effects of source mixing to be distinguished from biological fractionation.

4.2. Nitrogen attenuation

A mass-balance approach that combines $\delta^{15}\text{N-NH}_4^+$ and $\delta^{15}\text{N-NO}_3^-$ ($\delta^{15}\text{N-DIN}$) is an effective tool for identifying N attenuation activity in contaminated groundwater with complex chemistry (Izbicki et al., 2015). Variations in $\delta^{15}\text{N-DIN}$ distinguish internal cycling (NH_4^+ oxidation to NO_3^- , NO_3^- reduction to NH_4^+), which has an apparent ϵ of 0‰, from attenuation (NO_3^- reduction to N_2O and N_2 , NO_2^- reduction to N_2O and N_2 , NH_4^+ oxidation to N_2), which has an apparent ϵ of <0‰ (Table 1). As all biological attenuation processes preferentially convert ¹⁴N to gaseous N forms and increase the $\delta^{15}\text{N}$ value of the residual DIN pool (Table 1), all values of $\delta^{15}\text{N-DIN} > \delta^{15}\text{N}_0$ reflect *in-situ* biological attenuation (Izbicki, 2014). This approach avoids the weakness in using the relationship between $\delta^{15}\text{N-NO}_3^-$ and $[\text{NO}_3^-]$ to assess attenuation in NH_4^+ contaminated groundwater caused by the fact that the tightly coupled oxidation (NO_3^- production) and reduction (NO_3^- attenuation) effectively decouple $\delta^{15}\text{N-NO}_3^-$ from $[\text{NO}_3^-]$ (Hinkle et al., 2008; Meckenstock et al., 2015). Critically for a heterogeneous site, the DIN approach clarifies the compound-specific $\delta^{15}\text{N}$ variability at comparable low concentrations reported here (Figs. 4 and 5) by determining when shifts represent a change in the N

attenuation pathway rather than simply *in-situ* N recycling.

The difference between well $\delta^{15}\text{N-DIN}$ and the established $\delta^{15}\text{N}_0$ was used as a proxy for attenuation magnitude, as per Eq. (1) (Wells et al., 2016). Attenuation magnitude estimates were kept conservative by using each aquifer’s maximum, rather than mean, $\delta^{15}\text{N}_0$ value (i.e., all wells with $\delta^{15}\text{N-DIN}$ values < +5‰ in the chalk and < -10‰ in the sand aquifers show no significant N attenuation). These calculations assume that: 1) the apparent ϵ value for attenuation (ϵ_{atten}) is roughly constant across the site, and, 2) mixing is complete. With these assumptions, the aquifers’ $\delta^{15}\text{N-DIN}$ patterns can be treated as spatial ‘isoscapes’ (Bai et al., 2013). The site’s complex chemistry makes it particularly critical that this approach does not depend on knowledge of the biological attenuation pathways.

Only three wells in the sand aquifer (including the two source wells) and 20 wells in the chalk aquifer (including the five source wells) showed no evidence of attenuation (i.e., had $\delta^{15}\text{N-DIN} \leq \delta^{15}\text{N}_0$). ‘Non-attenuating’ wells in the chalk aquifer were primarily located in the North zone. In the sand aquifer all non-attenuating wells were located near the source area. Subsequently, $\delta^{15}\text{N-DIN} - \delta^{15}\text{N}_0$ increased over the flow path in both aquifers ($p < 0.01$, Fig. 6). This confirms the expectation that net attenuation increases as water flows away from the source plumes.

Mean $\delta^{15}\text{N-DIN} - \delta^{15}\text{N}_0$ values were greater in the sand aquifer than in the chalk ($19 \pm 10\%$ v. $4.3 \pm 5\%$, $p < 0.01$, after normalising all $\delta^{15}\text{N-DIN} \leq \delta^{15}\text{N}_0$ values to 0). The higher range of $\delta^{15}\text{N}_0$ values in the chalk aquifer affects these calculations: removing the highest $\delta^{15}\text{N}_0$ value from chalk aquifer calculations increased the mean $\delta^{15}\text{N-DIN} - \delta^{15}\text{N}_0$ difference to $6.8 \pm 5\%$. A more detailed characterisation of $\delta^{15}\text{N}_0$ would be needed to verify this evidence that NH_4^+ attenuation is greater in the sand aquifer than in the chalk aquifer. Although precision could be improved, here it is sufficient to say that N source and sink locations could be distinguished, and that biological processes were actively attenuating N contamination within both aquifers. Despite this uncertainty, $\delta^{15}\text{N-DIN}$

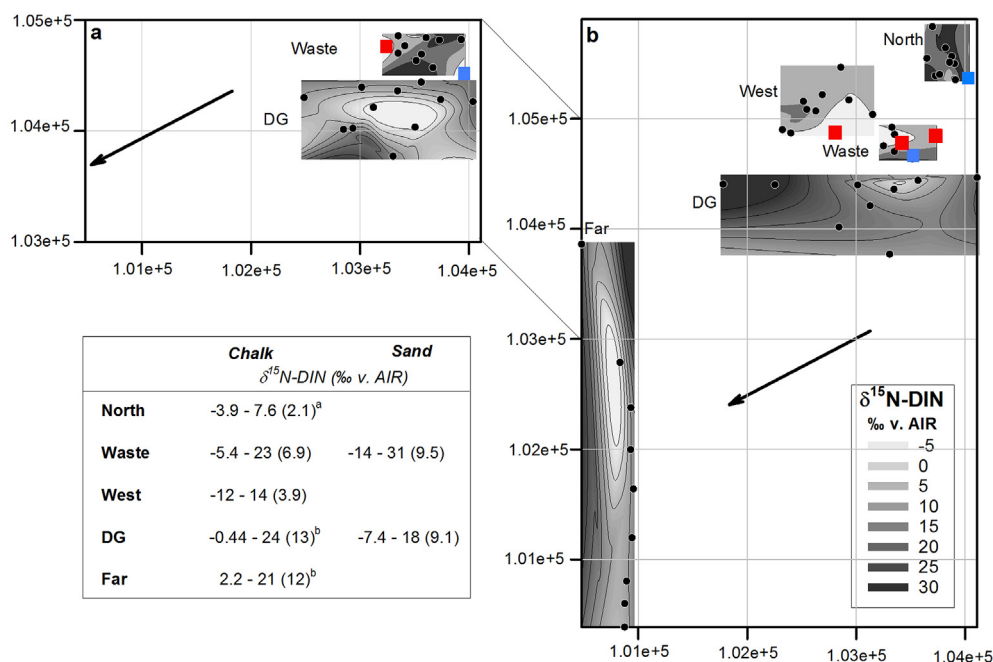


Fig. 6. Changes in $\delta^{15}\text{N}$ composition of DIN (concentration weighted mean of $\delta^{15}\text{N-NH}_4^+$, $\delta^{15}\text{N-NO}_3^-$, and $\delta^{15}\text{N-NO}_2^-$) across the sand (a) and chalk (b) aquifers underlying a historical industrial site in eastern Belgium. Circles indicate the 70 sampling wells, which were distributed from directly under the site (North, Waste, West) to further downgradient (dark colours). Black circles represent sampling well locations; hypothesised ‘source’ wells are marked with red (C1, S1) or blue (C2, S2) squares. Axes display arbitrary numbers that are 1:1 equivalent to UTM units, in accordance with site confidentiality agreements. (For interpretation of the references to colour in this figure legend, the reader is referred to the web version of this article.)

patterns indicate that N is attenuated more readily from the sand aquifer than from the chalk. Lower NO_3^- accumulation and narrower spatial cover by 'extreme' [DIN] found in the sand aquifer support this conclusion.

4.3. Attenuation pathways

The heterogeneous site chemistry makes it impossible to rule out any of the known N attenuation pathways: the high C and NO_3^- levels within the contaminated zone form an ideal environment for denitrification (Salminen et al., 2014), while high $[\text{NH}_4^+]$ and low $[\text{O}_2]$ near the source locations could favour anammox (Moore et al., 2011). Differentiating NH_4^+ removal from anammox v. nitrification-denitrification is complicated by the fact that they infer roughly identical fractionation patterns on the residual N-NH_x pool (Table 1). Some studies used a lack of NO_3^- accumulation following progressive $\delta^{15}\text{N-NH}_4^+$ enrichment as evidence that anammox, not nitrification, drives NH_4^+ removal (Clark et al., 2008; Robertson et al., 2012). However, this approach overlooks the fact that other biological attenuation pathways (nitrifier-denitrification) can oxidise NH_x without producing NO_3^- (Venterea et al., 2015). Even assuming that 'alternative' pathways are not involved, the fact that NO_3^- produced within NH_4^+ rich groundwater is often completely removed within narrow (cm scale) redox transition zones means that nitrification produced NO_3^- may not accumulate at a scale that would be reliably detected via routine groundwater sampling (Meckenstock et al., 2015; Spence et al., 2005). These issues with broad-scale isotopic assessments can be bypassed by instead focusing on functional pathways. Specifically, distinguishing heterotrophic NO_3^- reduction (denitrification) and autotrophic NO_2^- reduction (anammox, nitrifier-denitrification) dominated zones provides key information on the energetic controls on *in-situ* N attenuation, but avoids making any assumptions about the microbial communities involved.

4.3.1. Nitrate reduction

With the possibility of a significant independent NO_3^- source excluded, the fact that both $\delta^{18}\text{O-NO}_3^-$ and $\delta^{15}\text{N-NO}_3^-$ values in most wells were above the range possible from *in-situ* NO_3^- production must reflect NO_3^- reduction within the aquifers' N pools (Fig. 5). The data roughly fit the established fractionation pattern for NO_3^- reduction during denitrification (Fig. 5). Wells with the highest $[\text{NO}_3^-]$ have $\delta^{18}\text{O-NO}_3^-$ and $\delta^{15}\text{N-NO}_3^-$ values within the expected 'source' range, and both $\delta^{18}\text{O-NO}_3^-$ and $\delta^{15}\text{N-NO}_3^-$ increase in a roughly linear pattern from that zone (after excluding suspected fertiliser-affected wells: $x = 0.71$, $r^2 = 0.5$) indicates that variable rates of NO_3^- reduction are shaping the NO_3^- pool across the megasite (Wells et al., 2016). However, if reduction were the only process affecting the NO_3^- pool the fit of the $\delta^{18}\text{O-NO}_3^-$ v. $\delta^{15}\text{N-NO}_3^-$ relationship would be 1.0.

In natural environments co-occurring nitrification frequently affects the $\delta^{18}\text{O}:\delta^{15}\text{N}$ denitrification signature as the newly formed 'nitrified' NO_3^- pool mixes with the residual 'denitrified' NO_3^- pool: increasing nitrification relative to denitrification shifts the $\delta^{18}\text{O}:\delta^{15}\text{N}$ relationship from $1 \rightarrow 0$ (Wankel et al., 2009). The elevated $[\text{O}_2]$, [salt], $[\text{CN}^-]$, and/or [BTEX] could also drive variation in the $\delta^{18}\text{O}:\delta^{15}\text{N}$ enrichment ratio as stressed denitrifier community differentially fractionate NO_3^- dual isotopes (Kritee et al., 2012). However, the lack of systematic differences in NO_3^- isotopic composition across measured contaminant gradients makes it unlikely that cellular stress controlled $\delta^{18}\text{O}:\delta^{15}\text{N}$ variability at the whole-site scale. Furthermore, this large variation in redox conditions and oxide availability even within the most contaminated zones means that active nitrification could not be ruled out in any of the sampled locations. The presence of NH_4^+ in all sampled

locations and the non-continuous NO_3^- distribution across the site makes co-occurring nitrification the most likely explanation for the variations in NO_3^- isotopic composition from the expected 'reduction' line. The fact that the largest range in $\delta^{15}\text{N-NO}_3^-$ values was found between wells with comparably low $[\text{NO}_3^-]$ (Fig. 5) supports the hypothesis that oscillations between production-limited zones (low $[\text{NO}_3^-]$ with low $\delta^{15}\text{N-NO}_3^-$ values) and reduction dominated zones (low $[\text{NO}_3^-]$ with high $\delta^{15}\text{N-NO}_3^-$ values) drove NO_3^- isotopic variability across the aquifers (Hosono et al., 2013).

Notably, there are wells within the 'non-attenuating' portions of the Waste zone ($\delta^{15}\text{N-DIN} < \delta^{15}\text{N}_0$) that show evidence of NO_3^- reduction ($\delta^{18}\text{O-NO}_3^-$ and $\delta^{15}\text{N-NO}_3^-$ elevated along a roughly 1:1 ratio relative to the predicted $\delta^{15}\text{N}_0$ range). Wells with low $[\text{NO}_3^-]$ and relatively high $\delta^{18}\text{O}$ and $\delta^{15}\text{N}$ values within the source plumes of the chalk aquifer contributed to a lack of relationship between 'reduction' zones and location along the flow path, and indicates that either low levels of NH_4^+ nitrification and denitrification occur within the plumes. Nitrate reduction occurring within the $\delta^{15}\text{N}_0$ chalk locations would support the argument that the high variability in chalk $\delta^{15}\text{N}_0$ values stems from low levels of *in-situ* attenuation. This isotopic evidence for variable rates of N oxidation v. reduction across the entire site contrasts to the progressive $\delta^{15}\text{N}$ enrichment often reported for aquifers affected by a single plume or source (Izbicki, 2014; Singleton et al., 2007).

4.3.2. Nitrite reduction

Nitrite's rapid turnover (residence time of ~20 days even in nutrient poor marine O_2 minimum zones (Buchwald and Casciotti, 2013)) means that it can provide a snapshot of the activity actually occurring within the sampling location. This provides a useful contrast to $\delta^{15}\text{N-NH}_4^+$ and $\delta^{15}\text{N-NO}_3^-$ values, whose slower turnover means that they must be considered to reflect an integrated picture of processing up-gradient. Nitrite is produced (NH_3 oxidation) and consumed (NO_2^- oxidation) during nitrification, produced (NO_3^- reduction) and consumed (NO_2^- reduction) during denitrification, and consumed during anammox ($\text{NH}_4^+ + \text{NO}_2^- \rightarrow \text{N}_2$), meaning that it can drive N attenuation without accumulating appreciably in the environment (Dähnke and Thamdrup, 2013; Venterea et al., 2015).

$\delta^{15}\text{N-NO}_2^-$ is generally less enriched than either $\delta^{15}\text{N-NH}_4^+$ or $\delta^{15}\text{N-NO}_3^-$ as the combination of regular fractionation during NH_3 oxidation to NO_2^- and inverse fractionation during NO_2^- oxidation to NO_3^- cause $\delta^{15}\text{N-NO}_2^-$ to progressively decrease under nitrification dominated conditions, while denitrification produces NO_2^- that is lighter than the NO_3^- reactant, and NO_2^- reduction (via either heterotrophic denitrification or autotrophic anammox) increases $\delta^{15}\text{N-NO}_2^-$ (Fig. 7). Assuming that NO_2^- originated roughly at the sampling location, and thus that the measured $\delta^{15}\text{N-NH}_4^+$ and $\delta^{15}\text{N-NO}_3^-$ compositions of each well provide 'well specific' R_0 values for NO_2^- production/consumption, this information enabled $\delta^{15}\text{N-NO}_2^-$ to be used to elucidate the pathways affecting N turnover in each well.

Within the contaminated zones, five sand aquifer wells and four chalk aquifer wells had values of $\delta^{15}\text{N-NO}_2^- > \delta^{15}\text{N-NH}_4^+$, and an additional three chalk aquifer wells had values of $\delta^{15}\text{N-NO}_2^- \approx \delta^{15}\text{N-NH}_4^+$ (Fig. 7). All of these wells had $[\text{NO}_2^-]$ and $[\text{NH}_4^+]$ above the aquifer means ($p < 0.05$). Increasing $\delta^{15}\text{N-NO}_2^- - \delta^{15}\text{N-NH}_4^+$ was correlated with decreasing redox potential ($p < 0.05$) and increasing pH ($p < 0.05$) in the sand aquifer. The prevalence of wells with $\delta^{15}\text{N-NO}_2^- < \delta^{15}\text{N-NH}_4^+$ (Fig. 7) demonstrates the dominance of oxidation, rather than reduction, in controlling the size of the NO_2^- pool (Buchwald and Casciotti, 2013). $\delta^{15}\text{N-NO}_2^-$ tended to decrease relative to $\delta^{15}\text{N-NH}_4^+$ with increasing distance from the contaminant zone ($\delta^{15}\text{N-NO}_2^- - \delta^{15}\text{N-NH}_4^+$ was ~ -50‰ in the two Far zone locations with

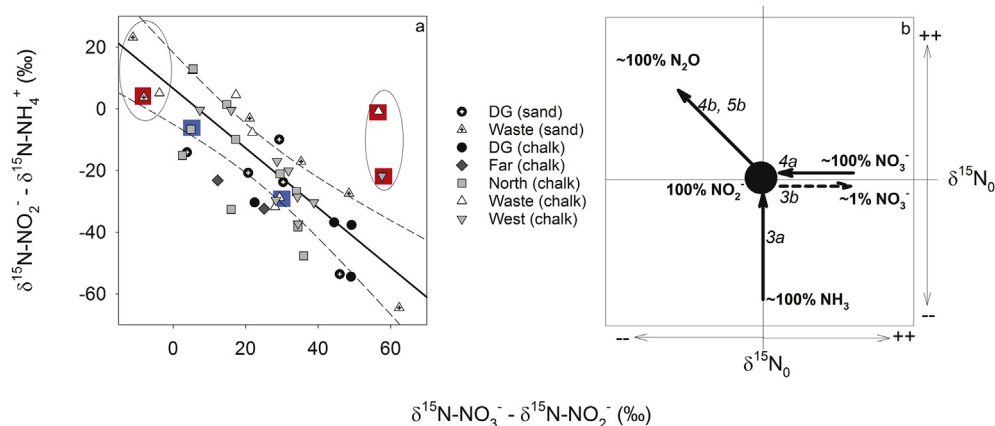


Fig. 7. The relationship between variations in $\delta^{15}\text{N-NO}_2^-$, $\delta^{15}\text{N-NH}_4^+$ and $\delta^{15}\text{N-NO}_3^-$ measured within a shallow sand aquifer and a deeper chalk aquifer underlying an industrial area in eastern Belgium (a). Samples were collected from a total of 70 wells across the two aquifers, but data is only shown here for locations where all three DIN species were detected (sand: $n = 14$; chalk: $n = 34$). The data is fit with a linear regression curve (solid line, dashed lines = 95% confidence intervals). The theoretical movement within this triple isotope space is shown in (b), where arrows indicate the expected patterns created by fractionation during NH_3 oxidation (3a), NO_2^- oxidation (3b), NO_3^- reduction (4a), and NO_2^- reduction (4b, 5b). Numbers and ϵ values correspond to those in Table 1. Circled points in (a) have $\delta^{15}\text{N}$ distribution outside of the range that readily explained by nitrification + denitrification; samples from hypothesised source wells are highlighted with either red (S1, C1) or blue (C2) squares. (For interpretation of the references to colour in this figure legend, the reader is referred to the web version of this article.)

detectable concentrations) (Table 3). This shift supports the increasing dominance of oxidation on N turnover downgradient from the contaminated zone that was anticipated based on the redox and O_2 profiles (Table 2).

Nitrite reduction, either autotrophic or heterotrophic, is the only process that can create values of $\delta^{15}\text{N-NO}_2^- > \delta^{15}\text{N-NH}_4^+$ (Fig. 7b). Thus the relatively elevated $\delta^{15}\text{N-NO}_2^-$ values within a few wells here provides compelling evidence that N attenuation occurs even within the most contaminated regions of both aquifers. The prevalence of NH_4^+ -rich wells with low $[\text{NO}_3^-]$ and high $\delta^{15}\text{N-NO}_3^- + \delta^{18}\text{O-NO}_3^-$ within the contaminant zones could be assumed to confirm that nitrification-limited denitrification drives N attenuation. However, high $[\text{NH}_4^+]$ can inhibit NO_2^- oxidation and increase autotrophic and/or chemical NO_2^- reduction (Venterea et al., 2015), both of which would produce the elevated $\delta^{15}\text{N-NO}_2^-$ values also found in NH_4^+ -rich wells.

The within-well relationship between $\delta^{15}\text{N-NO}_2^-$ and $\delta^{15}\text{N-NO}_3^-$ helped to clarify where NO_2^- reduction occurred via autotrophic v. heterotrophic pathways. During steady-state denitrification, the maximal difference between $\delta^{15}\text{N-NO}_3^-$ and $\delta^{15}\text{N-NO}_2^-$ is defined by their relative fractionation factors, $^{15}\epsilon_{\text{denit,NO}_3} - ^{15}\epsilon_{\text{denit,NO}_2}$ (Bourbonnais et al., 2015). Thus denitrification produces $\delta^{15}\text{N-NO}_3^-$ values between 30‰ and 0‰ greater than $\delta^{15}\text{N-NO}_2^-$ (depending on $^{15}\epsilon_{\text{denit}}$, Table 1), and coupling with nitrification is needed to farther increase this difference ($\delta^{15}\text{N-NO}_3^- - \delta^{15}\text{N-NO}_2^-$) to up to ~50‰ (Bourbonnais et al., 2015; Casciotti, 2009). Here, $\delta^{15}\text{N-NO}_3^- - \delta^{15}\text{N-NO}_2^-$ ranged from -11‰ to +62‰. Wells with negative values ($n = 3$) clustered around source C1/S1, had $\delta^{15}\text{N-NO}_2^- > \delta^{15}\text{N-NH}_4^+$, and had $[\text{NO}_2^-] > 0.1 \text{ mg N l}^{-1}$. These conditions support the hypothesis that NO_2^- accumulation is coupled with a direct NO_2^- reduction pathway within the NH_4^+ rich region of the site. The fact that these anomalous signatures were absent from the low pH source (C2/S2) corroborates evidence from the soil environment that direct NO_2^- reduction is a pH dependent process (Venterea et al., 2015). Fine-scale isotope measurements are recommended within these wells to provide a bottom-up constraint on the prevalence of direct NO_2^- reduction within the contaminant zone.

Outside of this narrow zone around C1/S1, $\delta^{15}\text{N}$ variations of each of the three measured DIN species reasonably fit the pattern expected for coupled nitrification and denitrification. In both

aquifers there was a linear relationship of $y = 6.6 - 0.97x$ ($r^2 = 0.78$; CI: 0.7, 1.2) between $\delta^{15}\text{N-NO}_2^- - \delta^{15}\text{N-NH}_4^+$ and $\delta^{15}\text{N-NO}_3^- - \delta^{15}\text{N-NO}_2^-$, such that $\delta^{15}\text{N-NO}_3^- + 0.03 \delta^{15}\text{N-NO}_2^- - \delta^{15}\text{N-NH}_4^+ = 6.6\text{‰}$. Thus if a pseudo-steady state is accepted, ϵ_{atten} across the site is -6.6‰ (Fig. 7). Consistent relationships between $\delta^{15}\text{N-NH}_4^+$, $\delta^{15}\text{N-NO}_2^-$, and $\delta^{15}\text{N-NO}_3^-$ both within each well and across the site demonstrate functional biogeochemical pathways across most of the site, despite the heterogeneous redox and contaminant chemistry. Thus despite evidence that autotrophic NO_2^- reduction occurs within the contaminated zone, coupled nitrification and denitrification control N attenuation at the regional scale.

5. Conclusion

We developed a multi-isotope approach capable of distinguishing N sources and sinks in a complex double aquifer system, which revealed nuances of N cycling within contaminated groundwater environments. Key outcomes include:

- Constraining $\delta^{15}\text{N}_0$ values and focusing on $\delta^{15}\text{N-DIN}$, rather than compound-specific dynamics, bypassed the difficulties caused by the wide fractionation range for the key N cycling processes.
- Evidence for autotrophic NO_2^- reduction processes within NH_4^+ plumes suggests that such zones can play a more active role in groundwater N attenuation than previously thought, although nitrification coupled to heterotrophic (or abiotic) denitrification drove N attenuation at the regional scale.
- Findings suggest that accurately predicting groundwater NH_4^+ fate is primarily limited by failing to fully capture redox fluctuations, and only secondly by failing to account for a role of autotrophic biological N attenuation pathways.
- Expanding isotope-based approaches beyond NO_3^- is here demonstrated to provide a uniquely empirical tool for constraining both the regional extent of N attenuation and the immediate biological processes that drive this attenuation.

Acknowledgements

Research was funded by the European Community's Seventh Framework Programme (FP7/2007–2013 under grant agreement

number 265063). **110** (47) VH acknowledge funding from the European Research Council through the project MHetScale (FP7-IDEAS-ERC-617511). Thanks to G. Bao and N. Fernandez de Vera for field assistance. Sampling and well access was possible thanks to S. Garzaniti (ISSEP), M. Lebel and P. Dengis (SPAQuE), and V. Lebrun (SPW-DGO3). The sampling campaign was initiated by J.A. Hernandez Peña.

Appendix A. Supplementary data

Supplementary data related to this article can be found at <http://dx.doi.org/10.1016/j.watres.2016.04.025>.

References

- Bai, E., Boutton, T.W., Liu, F., Wu, X.B., Archer, S.R., 2013. N-15 isoscapes in a subtropical savanna parkland: spatial-temporal perspectives. *Ecosphere* 4 (1), 17.
- Bourbonnais, A., Altabet, M.A., Charoenpong, C.N., Larkum, J., Hu, H., Bange, H.W., Stramma, L., 2015. N-loss isotope effects in the Peru oxygen minimum zone studied using a mesoscale eddy as a natural tracer experiment. *Glob. Biogeochem. Cy.* 29 (6), 793–811.
- Brunner, B., Contreras, S., Lehmann, M.F., Matantseva, O., Rollog, M., Kalvelage, T., Klockgether, G., Lavik, G., Jetten, M.S.M., Kartal, B., Kuypers, M.M.M., 2013. Nitrogen isotope effects induced by anammox bacteria. *Proc. Natl. Acad. Sci. U. S. A.* 110 (47), 18994–18999.
- Bryan, B.A., Shearer, G., Skeeters, J.L., Kohl, D.H., 1983. Variable expression of the nitrogen isotope effect associated with denitrification of nitrite. *J. Biol. Chem.* 258 (14), 8613–8617.
- Buchwald, C., Casciotti, K.L., 2013. Isotopic ratios of nitrite as tracers of the sources and age of oceanic nitrite. *Nat. Geosci.* 6 (4), 308–313.
- Burgin, A.J., Hamilton, S.K., 2008. NO_3^- -driven SO_4^{2-} production in freshwater ecosystems: implications for N and S Cycling. *Ecosystems* 11 (6), 908–922.
- Casciotti, K.L., 2009. Inverse kinetic isotope fractionation during bacterial nitrite oxidation. *Geochim. Cosmochim. Acta* 73 (7), 2061–2076.
- Casciotti, K.L., Bohlke, J.K., McIlvin, M.R., Mroczkowski, S.J., Hannon, J.E., 2007. Oxygen isotopes in nitrite: analysis, calibration, and equilibration. *Anal. Chem.* 79 (6), 2427–2436.
- Casciotti, K.L., Sigman, D.M., Hastings, M.G., Bohlke, J.K., Hilkert, A., 2002. Measurement of the oxygen isotopic composition of nitrate in seawater and freshwater using the denitrifier method. *Anal. Chem.* 74 (19), 4905–4912.
- Casciotti, K.L., Sigman, D.M., Ward, B.B., 2003. Linking diversity and stable isotope fractionation in ammonia-oxidizing bacteria. *Geomicrobiol. J.* 20 (4), 335–353.
- Clague, J.C., Stenger, R., Clough, T.J., 2015. Evaluation of the stable isotope signatures of nitrate to detect denitrification in a shallow groundwater system in New Zealand. *Agric. Ecosyst. Environ.* 202 (0), 188–197.
- Clark, I., Timlin, R., Bourbonnais, A., Jones, K., Lafleur, D., Wickens, K., 2008. Origin and fate of industrial ammonium in anoxic ground water – (15)N evidence for anaerobic oxidation (anammox). *Ground Water Monit. Remed.* 28 (3), 73–82.
- Colliver, B.B., Stephenson, T., 2000. Production of nitrogen oxide and dinitrogen oxide by autotrophic nitrifiers. *Biotechnol. Adv.* 18 (3), 219–232.
- Dähnke, K., Thamdrup, B., 2013. Nitrogen isotope dynamics and fractionation during sedimentary denitrification in Boknis Eck, Baltic Sea. *Biogeosciences* 10 (5), 3079–3088.
- Dhondt, K., Boeckx, P., Van Cleemput, O., Hofman, G., 2003. Quantifying nitrate retention processes in a riparian buffer zone using the natural abundance of N-15 in NO_3^- . *Rapid Commun. Mass Spectrom.* 17 (23), 2597–2604.
- Fang, Y.T., Koba, K., Makabe, A., Takahashi, C., Zhu, W.X., Hayashi, T., Hokari, A.A., Urakawa, R., Bai, E., Houlton, B.Z., Xi, D., Zhang, S.S., Matsushita, K., Tu, Y., Liu, D.W., Zhu, F.F., Wang, Z.Y., Zhou, G.Y., Chen, D.X., Makita, T., Toda, H., Liu, X.Y., Chen, Q.S., Zhang, D.Q., Li, Y.D., Yoh, M., 2015. Microbial denitrification dominates nitrate losses from forest ecosystems. *Proc. Natl. Acad. Sci. U. S. A.* 112 (5), 1470–1474.
- Fenech, C., Rock, L., Nolan, K., Tobin, J., Morrissey, A., 2012. The potential for a suite of isotope and chemical markers to differentiate sources of nitrate contamination: a review. *Water Res.* 46 (7), 2023–2041.
- Galloway, J.N., Aber, J.D., Erisman, J.W., Seitzinger, S.P., Howarth, R.W., Cowling, E.B., Cosby, B.J., 2003. The nitrogen cascade. *Bioscience* 53 (4), 341–356.
- Goody, D.C., Macdonald, D.M.J., Lapworth, D.J., Bennett, S.A., Griffiths, K.J., 2014. Nitrogen sources, transport and processing in pen-urban floodplains. *Sci. Total Environ.* 494, 28–38.
- Granger, J., Sigman, D.M., Lehmann, M.F., Tortell, P.D., 2008. Nitrogen and oxygen isotope fractionation during dissimilatory nitrate reduction by denitrifying bacteria. *Limnol. Oceanogr.* 53 (6), 2533–2545.
- Griebler, C., Avramov, M., 2015. Groundwater ecosystem services: a review. *Freshw. Sci.* 34 (1), 355–367.
- Hatzinger, P.B., Bohlke, J.K., Sturchio, N.C., 2013. Application of stable isotope ratio analysis for biodegradation monitoring in groundwater. *Curr. Opin. Biotechnol.* 24 (3), 542–549.
- Hinkle, S.R., Bohlke, J.K., Fisher, L.H., 2008. Mass balance and isotope effects during nitrogen transport through septic tank systems with packed-bed (sand) filters. *Sci. Total Environ.* 407 (1), 324–332.
- Hinkle, S.R., Tesoriero, A.J., 2014. Nitrogen speciation and trends, and prediction of denitrification extent, in shallow US groundwater. *J. Hydrol.* 509, 343–353.
- Hood, J.L.A., Taylor, W.D., Schiff, S.L., 2014. Examining the fate of WWTP effluent nitrogen using delta N-15-NH4 (+), delta N-15-NO (3) (-) and delta N-15 of submersed macrophytes. *Aquat. Sci.* 76 (2), 243–258.
- Hosono, T., Tokunaga, T., Kagabu, M., Nakata, H., Orishikida, T., Lin, I.T., Shimada, J., 2013. The use of delta15N and delta18O tracers with an understanding of groundwater flow dynamics for evaluating the origins and attenuation mechanisms of nitrate pollution. *Water Res.* 47 (8), 2661–2675.
- Izbicki, J.A., 2014. Fate of nutrients in shallow groundwater receiving treated septage, Malibu, CA. *Groundwater* 52, 218–233.
- Izbicki, J.A., Flint, A.L., O'Leary, D.R., Nishikawa, T., Martin, P., Johnson, R.D., Clark, D.A., 2015. Storage and mobilization of natural and septic nitrate in thick unsaturated zones, California. *J. Hydrol.* 524, 147–165.
- Jones, L.C., Peters, B., Lezama Pacheco, J.S., Casciotti, K.L., Fendorf, S., 2015. Stable isotopes and iron oxide mineral products as markers of chemodenitrification. *Environ. Sci. Technol.* 49 (6), 3444–3452.
- Karthic, I., Brugam, R.B., Retzlaff, W., Johnson, K., 2013. The impact of nitrogen contamination and river modification on a Mississippi River floodplain lake. *Sci. Total Environ.* 463, 734–742.
- Kellogg, D.Q., Gold, A.J., Groffman, P.M., Addy, K., Stolt, M.H., Blazejewski, G., 2005. In situ ground water denitrification in stratified, permeable soils underlying riparian wetlands. *J. Environ. Qual.* 34 (2), 524–533.
- Kleinsteuber, S., Schleinitz, K.M., Vogt, C., 2012. Key players and team play: anaerobic microbial communities in hydrocarbon-contaminated aquifers. *Appl. Microbiol. Biotechnol.* 94 (4), 851–873.
- Klove, B., Ala-Aho, P., Bertrand, G., Gurdak, J.J., Kupfersberger, H., Kvaerner, J., Muotka, T., Mykra, H., Preda, E., Rossi, P., Uvo, C.B., Velasco, E., Pulido-Velazquez, M., 2014. Climate change impacts on groundwater and dependent ecosystems. *J. Hydrol.* 518, 250–266.
- Koh, D.C., Mayer, B., Lee, K.S., Ko, K.S., 2010. Land-use controls on sources and fate of nitrate in shallow groundwater of an agricultural area revealed by multiple environmental tracers. *J. Contam. Hydrol.* 118 (1–2), 62–78.
- Kool, D.M., Wrage, N., Zechmeister-Boltenstern, S., Pfeffer, M., Brus, D., Oenema, O., Van Groenigen, J.W., 2010. Nitrifier denitrification can be a source of N_2O from soil: a revised approach to the dual-isotope labelling method. *Eur. J. Soil Sci.* 61 (5), 759–772.
- Kritee, K., Sigman, D.M., Granger, J., Ward, B.B., Jayakumar, A., Deutsch, C., 2012. Reduced isotope fractionation by denitrification under conditions relevant to the ocean. *Geochim. Cosmochim. Acta* 92, 243–259.
- Mariotti, A., Germon, J.C., Hubert, P., Kaiser, P., Letolle, R., Tardieux, A., Tardieux, P., 1981. Experimental determination of nitrogen kinetic isotope fractionation – some principles – illustration for the denitrification and nitrification processes. *Plant Soil* 62 (3), 413–430.
- Marliere, R., 1977. Livret explicatif de la feuille Beloeil-Baudour 139 de la carte géologique au 1/25000. Service Géologique Belge.
- McIlvin, M.R., Altabet, M.A., 2005. Chemical conversion of nitrate and nitrite to nitrous oxide for nitrogen and oxygen isotopic analysis in freshwater and seawater. *Anal. Chem.* 77 (17), 5589–5595.
- McIlvin, M.R., Casciotti, K.L., 2011. Technical updates to the bacterial method for nitrate isotopic analyses. *Anal. Chem.* 83 (5), 1850–1856.
- Meckenstock, R.U., Elsner, M., Griebler, C., Lueders, T., Stumpp, C., Aamand, J., Agathos, S.N., Albrechtsen, H.J., Bastiaens, L., Bjerg, P.L., Boon, N., Dejonghe, W., Huang, W.E., Schmidt, S.I., Smolders, E., Sorensen, S.R., Springael, D., van Breukelen, B.M., 2015. Biodegradation: updating the concepts of control for microbial cleanup in contaminated aquifers. *Environ. Sci. Technol.* 49 (12), 7073–7081.
- Moore, T.A., Xing, Y., Lazenby, B., Lynch, M.D., Schiff, S., Robertson, W.D., Timlin, R., Lanza, S., Ryan, M.C., Aravena, R., Fortin, D., Clark, I.D., Neufeld, J.D., 2011. Prevalence of anaerobic ammonium-oxidizing bacteria in contaminated groundwater. *Environ. Sci. Technol.* 45 (17), 7217–7225.
- Murgulet, D., Tick, G.R., 2013. Understanding the sources and fate of nitrate in a highly developed aquifer system. *J. Contam. Hydrol.* 155, 69–81.
- Ponsin, V., Coulomb, B., Guelorget, Y., Maier, J., Hohener, P., 2014. In situ biostimulation of petroleum hydrocarbon degradation by nitrate and phosphate injection using a dipole well configuration. *J. Contam. Hydrol.* 171, 22–31.
- Rivett, M.O., Buss, S.R., Morgan, P., Smith, J.W., Bemment, C.D., 2008. Nitrate attenuation in groundwater: a review of biogeochemical controlling processes. *Water Res.* 42 (16), 4215–4232.
- Robertson, W.D., Moore, T.A., Spoelstra, J., Li, L., Elgood, R.J., Clark, I.D., Schiff, S.L., Aravena, R., Neufeld, J.D., 2012. Natural attenuation of septic system nitrogen by anammox. *Ground Water* 50 (4), 541–553.
- Salminen, J.M., Petajajarvi, S.J., Tuominen, S.M., Nysten, T.H., 2014. Ethanol-based in situ bioremediation of acidified, nitrate-contaminated groundwater. *Water Res.* 63, 306–315.
- Sebilo, M., Billen, G., Grably, M., Mariotti, A., 2003. Isotopic composition of nitrate-nitrogen as a marker of riparian and benthic denitrification at the scale of the whole Seine River system. *Biogeochemistry* 63 (1), 35–51.
- Selbie, D.R., Lanigan, G.J., Laughlin, R.J., Di, H.J., Moir, J.L., Cameron, K.C., Clough, T.J., Watson, C.J., Grant, J., Somers, C., Richards, K.G., 2015. Confirmation of co-denitrification in grazed grassland. *Sci. Rep.* 5, 17361.
- Service Publique de Wallonie, 2006. Notice explicative de la masse d'eau souterraine RWE030.
- Singleton, M.J., Esser, B.K., Moran, J.E., Hudson, G.B., McNab, W.W., Harter, T., 2007.

- Saturated zone denitrification: potential for natural attenuation of nitrate contamination in shallow groundwater under dairy operations. *Environ. Sci. Technol.* 41 (3), 759–765.
- Sonthiphand, P., Hall, M.W., Neufeld, J.D., 2014. Biogeography of anaerobic ammonia-oxidizing (anammox) bacteria. *Front. Microbiol.* 5, 14.
- Spence, M.J., Bottrell, S.H., Thornton, S.F., Richnow, H.H., Spence, K.H., 2005. Hydrochemical and isotopic effects associated with petroleum fuel biodegradation pathways in a chalk aquifer. *J. Contam. Hydrol.* 79 (1–2), 67–88.
- Sutka, R.L., Ostrom, N.E., Ostrom, P.H., Gandhi, H., Breznak, J.A., 2003. Nitrogen isotopomer site preference of N₂O produced by *Nitrosomonas europaea* and *Methylococcus capsulatus* Bath. *Rapid Commun. Mass Spectrom.* 17 (7), 738–745.
- Sutka, R.L., Ostrom, N.E., Ostrom, P.H., Gandhi, H., Breznak, J.A., 2004. Nitrogen isotopomer site preference of N₂O produced by *Nitrosomonas europaea* and *Methylococcus capsulatus* Bath (vol 18, pg 1411, 2004). *Rapid Commun. Mass Spectrom.* 18 (12), 1411–1412.
- Venterea, R.T., Clough, T.J., Coulter, J.A., Breuillin-Sessoms, F., 2015. Ammonium sorption and ammonia inhibition of nitrite-oxidizing bacteria explain contrasting soil N₂O production. *Sci. Rep.* 5.
- Wankel, S.D., Kendall, C., Paytan, A., 2009. Using nitrate dual isotopic composition (delta N-15 and delta O-18) as a tool for exploring sources and cycling of nitrate in an estuarine system: Elkhorn Slough, California. *J. Geophys. Res. Biogeosci.* 114, 15.
- Wells, N.S., Baisden, W.T., Horton, T., Clough, T.J., 2016. Spatial and temporal variations in nitrogen export from a New Zealand pastoral catchment revealed by stream water nitrate isotopic composition. *Water Resour. Res.* 52 <http://dx.doi.org/10.1002/2015WR017642>.
- Xue, D., Botte, J., De Baets, B., Accoe, F., Nestler, A., Taylor, P., Van Cleemput, O., Berglund, M., Boeckx, P., 2009. Present limitations and future prospects of stable isotope methods for nitrate source identification in surface- and groundwater. *Water Res.* 43 (5), 1159–1170.
- Zhang, L., Altabet, M.A., Wu, T.X., Hadas, O., 2007. Sensitive measurement of (NH₄+N)-N-15/N-14 (delta(NH₄+)-N-15) at natural abundance levels in fresh and saltwaters. *Anal. Chem.* 79 (14), 5297–5303.